Quantification of the local protein content in hydrogels undergoing swelling and dissolution at alkaline pH using fluorescence microscopy

Weiji Liu[a], D. Ian Wilson[b], Xiao Dong Chen[a], Ruben Mercadé-Prieto[a*]

[a] Suzhou Key Laboratory of Green Chemical Engineering, School of Chemical and Environmental Engineering, College of Chemistry, Chemical Engineering and Materials Science, Soochow University, Suzhou City, Jiangsu 215123, P.R. China

[b] Department of Chemical Engineering and Biotechnology, University of Cambridge, Philippa Fawcett Drive, Cambridge, CB3 OAS, UK

* Email: ruben@suda.edu.cn

Abstract:

Wide-field fluorescence microscopy was used to quantify the evolution of the volumetric swelling ratio, *Q*, *i.e.* solids content, in a protein hydrogel undergoing swelling and dissolution. Heat-induced whey protein hydrogels labelled with Rhodamine B isothiocyanate (RITC) were used as a model system. Complications in the quantification of *Q* using fluorescence of proteins conjugated RITC, arising from alkali destroying protein-dye interactions, were overcome using a reaction-diffusion numerical scheme. At pH 12-13, when the hydrogels dissolve readily, overlapping fluorescence intensity profiles were observed at different times, consistent with a system dissolving at steady state. In stronger alkali (*e.g.* 1 M NaOH), when dissolution proceeds very slowly, we confirm that there is little swelling next to the gel boundary. These results present the first quantification of the solids distribution within protein hydrogels under reactive conditions.

Key words: dissolution; Rhodamine B isothiocyanate; volumetric swelling ratio; whey protein hydrogels.

1. Introduction

The capability of globular proteins to form hydrogels when heated is exploited in the food industry in the manufacturing of functional products (Shewan and Stokes 2014), but is simultaneously unwelcome in food manufacturing processes where it can lead to extensive fouling, typically in heat exchangers (Blanpain-Avet et al. 2016), which is responsible for several industrial issues, such as heat exchange reduction due to an additional thermal resistance (Mahdi et al. 2009), high pressure drop owing to hydrodynamic diameter decrease (Grijspeerdt et al. 2004), and biocontaminations (Fryer et al. 2006).

Protein fouling deposits in industry are usually cleaned by the circulation of alkaline solutions in cleaning-in-place (CIP) operations (Alvarez et al. 2010). Despite the ubiquity of this cleaning problem, for example in the dairy industry where CIP is practiced on a daily basis, a coherent and quantitative understanding of the mechanisms involved is incomplete due to its complexity. For instance, protein gels swell when in contact with an alkaline solution: if the pH is high enough, both weak and strong chemical interactions are cleaved, allowing the hydrogels to swell further, rendering them weak so that erosion can occur and, eventually, dissolve (Mercadé-Prieto et al. 2008b). Extensive swelling has been suggested to help the removal of proteinaceous deposits as it allows small oligomers to diffuse through the swollen layer (Mercadé-Prieto et al. 2008b). Quantitative modelling of this process has been hampered, however, by the difficulty in quantifying, experimentally, the local spatial swelling ratio (or the protein concentration) of a hydrogel undergoing swelling or dissolution. Detailed mechanistic models for verification of the underlying science and optimization of CIP processes require such information.

The swelling behavior of hydrogels has been investigated both experimentally and theoretically (English et al. 1996; Ganji et al. 2010), as it often controls the release

behavior of solvents and drugs from polymeric networks (Ganji and Vasheghani-Farahani 2009; Lin and Metters 2006). Techniques that have been applied to assess the progression of swelling include X-ray microtomography (XμT; Laity et al. 2010; Laity and Cameron 2010), atomic force microscopy (AFM; Govedarica et al. 2012; Paredes et al. 2006), magnetic resonance imaging (MRI; Oztop et al. 2010; Richardson et al. 2005), or terahertz-pulsed imaging (TPI; Yassin et al. 2015). A review of these techniques has been presented by Huanbutta et al. (2013).

Fluorescence microscopy represents a cheaper alternative to the above techniques for obtaining this localised information. For instance, pyrene and dansyl dyes have been used to investigate the swelling and shrinking behavior of hydrogels using steady-state fluorescence as they are sensitive to the microenvironment, *i.e.* solvent polarity (Tari and Pekcan 2011). Raccis et al. (2011) employed fluorescence correlation spectroscopy to investigate the mobility of tracer molecules in a thermoresponsive hydrogel film. Quantitative studies are more challenging. Wagner et al. (2016) monitored the swelling and deswelling of polyacrylamide hydrogel using simultaneous neutron, fluorescence and optical brightfield transmission imaging. In a recent study we quantified the swelling of disc-shaped Rhodamine B isothiocyanate (RITC)-labelled whey protein hydrogels at pH $\leq$ 11 using a conventional wide-field fluorescence microscope (Liu et al. 2017). The results showed that the fluorescence intensity of the hydrogels decreased as expected for isotropic swelling at pH $\leq$11, when dissolution occurs very slowly, if at all.

In this paper we report the use of the same wide-field microscopy (WFM) technique to quantify, for the first time, the local swelling ratio of whey protein gels dissolving at higher pH. An important difference is the use of samples formed within narrow cuvettes (of cross-section 1 mm × 10 mm) rather than the discs employed by Liu et al. (2017) as this greatly helps in the identification of the gel-solution boundary and interpretation of fluorescence intensity data. A second aspect of technique development is the use of a model-based approach to account for changes in fluorescence intensity caused by breakdown of protein-dye interactions at higher pH.

2. Experimental procedure

2.1 Materials and gel preparation

The protocol to prepare RITC-labelled whey protein gels (denoted WPI-RITC) was reported previously (Liu et al. 2017). In brief, a 2 wt% solution of whey protein isolate (WPI; Davisco, USA) in MilliQ water was homogenized and mixed with 2% (v/v) RITC (Exciton, USA) stock solution (~20 mM). The pH of the solution was adjusted to 9 by adding 1 M NaOH (aq) to prevent protonation of the amine group without denaturing the protein (Taulier and Chalikian 2001). The solution was held at room temperature under mild stirring for at least 16.5 h to reach maximum labelling. Dialysis was then performed to remove the unreacted RITC aseptically using a 6-8 kDa MWCO membrane (Spectra Laboratories) against 0.02% (w/v) sodium azide solution. The concentration of WPI and of RITC inside the membrane was monitored by UV/Vis absorption at 280 nm and 555 nm, respectively (SpectraMax M5, Molecular Devices). Dialysis was normally stopped after 65 h, which typically resulted in a solution with concentrations of ~1.3 wt% WPI and ~0.1 mM RITC. The low dye-protein ratio was used to minimize the conformational changes of the protein due to labelling (Hungerford et al. 2007).

The protein concentration of the dialyzed solution is too low to form a gel, so native WPI powder was added to achieve a WPI concentration of 15 wt% with a final RITC concentration of ~20 µM. Heat-induced WPI-RITC hydrogels were formed by heating 400 µL aliquots of WPI-RITC solution inside glass cuvettes (dimensions 1 mm × 10 mm, 45 mm tall) in a water bath for 30 min at 80 °C. In order to minimize the formation of bubbles in the gel, solutions were degassed for at least 1 h at ~0.01 MPa and 40 °C before heat treatment. After cooling to room temperature the gels were stored at 4 °C overnight; they were allowed to equilibrate to room temperature for at least one hour before testing.

2.2 Swelling and dissolution of WPI-RITC gels

The swelling and dissolution of protein hydrogels prepared inside the cuvettes was studied at room temperature using similar protocols to those reported elsewhere (Mercadé-Prieto and Chen 2006). Each cuvette was immersed in a well-mixed solution at the desired pH at room temperature and removed at selected times for imaging. Imaging took 10 min or less, after which the cuvette was returned to the solution.

2.3 Fluorescence measurement with WFM

Fluorescence measurements were performed using the equipment and procedure reported by Liu et al. (2017). In brief, a wide-field fluorescence microscope (MacroZoom Z16, Leica) with a 1.0× planapochromatic objective (magnification 7.13× – 115×) was used. The RITC was excited at wavelength of 530 nm (520-550 nm band, LED4D067, Thorlabs) and its fluorescence emission was recorded as 8 bit images with a monochrome CCD camera (ICX285ALCCD, ToupTek, 1360×1024 pixels, chip size 6.45 μm).

The main area of interest in studying swelling and dissolution is the 'swollen layer' adjacent to the gel-solution boundary. Determining the location of this boundary using WFM is problematic because gels cannot be formed with flat perpendicular boundaries inside cuvettes, due to capillary forces promoting wall wetting (see Figure 1(b)). The cuvette surface could theoretically be coated to minimize the wall effect but this was not attempted here. As WFM can only provide reliable data when the gel thickness is known, the approach developed to estimate the location where the gel thickness is constant (*i.e.* where the gel fills the gap between the cuvette walls, denoted the constant gel thickness boundary, CGB), is explained below.

Figure 1(a) shows that the strong reflection at the gel interface when imaged dry, which affects the fluorescence intensity in this region, is avoided when the cuvette was submerged in a petri dish with water during imaging. The CGB is not visible in immersed images so the surface reflection in air was used to locate the CGB, using a high grey threshold value, as shown in Figure 1(*c*). It should be noted that the

immersion step generates an artefact when studying the gel in its initially formed state, as the intensity at the boundary is slightly lower than that of the interior due to the ingress of some water.

All images were obtained at the lowest magnification (*i.e.* 7.13×) to maximize the field of view, typically needing 4 images to capture the length of the gel in the cuvette (approximately 44 mm). Matlab® was used for image processing, including alignment, image-merging and cropping of the 4 images (described in detail in Supplementary Information, Figure S1). In order to minimize edge effects, only the central 8 mm region of the gel was considered for analysis. Measurements were performed in darkness to get high signal-to-noise ratios: the typical background noise was a grey value of ~0.23 per second of exposure time using an unlabeled WPI gel.

2.4 Determination of the swelling ratio

The overall volumetric swelling ratio, Q_o, defined as the reciprocal of the protein volume fraction, $\phi_{2,s}$, was calculated from the total masses of the initial and the swollen gel, m_0 and m_{sw}, respectively (Mercadé-Prieto et al. 2007a):

$$Q_o = \frac{1}{\phi 2,s} = 1 + \frac{\upsilon_{sp,1}}{\upsilon_{sp,2}}\left(\frac{1}{w}\frac{m_{sw}}{m_0} - 1\right) \quad (1)$$

where $\upsilon_{sp,1}$ and $\upsilon_{sp,2}$ are the specific volumes of the solvent (*i.e.* water) and the protein (taken as 0.75×10^{-3} m^3 kg^{-1}) (Taulier and Chalikian 2001), respectively. w is the weight fraction of protein in the initial gel. The value of Q_o at formation, calculated with $m_{sw} = m_0$ and denoted Q_r, is used as the reference state.

Gel swelling is constrained in two dimensions by the cuvette walls. Assuming constant gel density, width, thickness, dye stability and no dye leakage, the fluorescence decrease due to 1D swelling is given by:

$$\frac{m_{sw}}{m_0} = \frac{V_{sw}}{V_0} = \frac{I_{WFM0}}{I_{WFM,sw}} \quad (2)$$

where I_{WFM0} and $I_{WFM,sw}$ are the fluorescence intensities of the initial and swollen gel, respectively. Consequently, the local swelling ratio of the hydrogel, Q, can be calculated from the local intensity via:

$$Q = 1 + \frac{\upsilon_{sp,1}}{\upsilon_{sp,2}}\left(\frac{1}{w}\left(\frac{I_{WFM,sw}}{I_{WFM0}}\right)^{-1} - 1\right) \quad (3)$$

2.5 Stability of WPI-RITC fluorescence in alkali

The fluorescence intensity at a constant protein labelled RITC concentration of 7.5 µM was measured with addition of different native WPI concentrations, ranging from 0.75 to 15 wt%, at alkaline pH. As small volumes were used, the amount of NaOH (aq.) required to achieve the desired pH was calculated using the hydrogen ion equilibrium curve (Zhao et al. 2016). After mixing for 30 s, an aliquot was placed in a petri dish for fluorescence measurements for 2.5 h. In control tests, MilliQ water was added instead of alkali.

2.6 Statistical Analysis

The sigmoidal regressions were evaluated using the SigmaPlot v12.5 (Systat, Software, Inc., USA). Welch t-tests were applied to check if fluorescence intensity profiles were statistically the same.

3. Results and Discussions

3.1 Initial protein gels

Figure 2 shows the fluorescence profiles obtained for two gel samples before contact with solution: the insets show the images after illumination correction (see Figure S2) and image processing. Gel 1 contains some bubbles and water droplets whereas Gel 2 was free from such inhomogeneities. The gels were prepared using same degassing protocol and demonstrates the need for care in preparing the gels.

Gel 2 shows homogeneous intensity except at the boundary, where a peak is evident. The peak is generated by local dehydration at the boundary during storage, causing the

gel to shrink. In contrast, large fluctuations of the fluorescence intensity were observed in Gel 1 due to the bubbles and droplets. The two profile calculation methods show that the median value is more robust towards bubbles (see Figure S3: this supplementary Figure also shows that the variability in $I_{WFM0,}$ from 12 repeats, was about 5%). The cuvettes are effectively identical (1.08 ± 0.01 mm thick) so this variation is attributed to small variations in RITC content between cuvettes and temperature fluctuations known to affect Rhodamine B fluorescence (Natrajan and Christensen 2009).

3.2 Velocity of the CGB during swelling and dissolution

The WFM technique allows the location of the CGB to be monitored and the velocity of this boundary, U_{BD}, to be estimated at different times. U_{BD} values for 15 wt% WPI-RITC gels submerged at different pH are plotted in Figure 3. Swelling (negative U_{BD}) is evident for all pH over the first ~1-2 h, changing to dissolution thereafter. The absolute value of U_{BD} decreases at pH 12-13, which is evident in the inset: these are also conditions which give rise to high dissolution rates (see Figure 4).

At longer times, U_{BD} approaches a roughly constant value, indicating that the dissolution rate is constant with time, which is consistent with many previous studies employing different techniques (Pérez-Mohedano et al. 2015). At high pH, U_{BD} decreases and is close to zero at pH 14, indicating an inhibited dissolution process. The constant dissolution rate velocities at pH 12-13 compare reasonably well with the penetration velocity of hydroxyl ion in BLG (β-lactoglobulin) or WPC (whey protein concentrate) gels reported previously (Mercadé-Prieto et al. 2008b; Mercadé-Prieto and Chen 2006). Figure 4 likewise shows that the estimated dissolution rates are in good agreement with directly measured rates reported previously.

3.3 Swelling at pH 11

Dissolution is slow at pH 11 and Figure 5 shows that extensive swelling is observed over a timescale of a few hours. In this case the experiment was terminated after 4.65

h as the CGB had emerged from the cuvette so swelling was no longer one dimensional. The solids content in the gel near the CGB is so low that it is difficult to distinguish it from the background. The images also show inhomogeneous swelling at the boundary, driven by the wall layer, and the appearance of holes after 1.65 h, particularly when the swelling is extensive (Figure S4). The effect of these defects was restricted by considering only the central 8 mm band in the calculations and the median intensity.

The profiles in Figure 6(*a*) show uniform fluorescence intensity at the initial state, with the CGB located about 8 mm from the cuvette entrance. The intensity does not change over time in the gel fraction distant from the boundary (> 15 mm), consistent with no ingress of solution there. These results demonstrate that the RITC-labelled gel is sufficiently stable for reliable quantification.

Nearer the boundary the fluorescence intensity decreases as the gel swells. The profiles show similar values in the region near the CGB boundary, up to ~2 mm deep, which is confirmed in the insets where the data are plotted against depth into the gel. Further into the gel, the intensity decreases steadily with time. The corresponding Q values in Fig. 6(*b*) show high values at the CGB, decreasing to the initial value of ~9.4 in the unswollen region. These are all consistent with progressive swelling driven by the diffusion of OH^- into the gel: these data represent the first direct measurements of the dynamic response to immersion in alkali. The Q value at the CGB approaches a steady value of 220 ± 40, which is in good agreement with the final Q_o value of ~200 obtained for disc-shaped gel samples (Liu et al. 2017).

3.4 *Fast dissolution (pH 12-13)*

Both the dissolution rate and the depth of penetration of OH^- into to the gel are known to be constant with time at pH 12-13 (Mercadé-Prieto et al. 2008a), indicating that the process is at steady state. The swollen layer is therefore expected to exhibit self-similar profiles in fluorescence intensity (and Q). The profiles in Figure 7 show considerable overlap and are statistically the same ($p>0.05$, Figure S5) despite there being extensive dissolution, as indicated by U_{BD} in Figure 3 and the position of the CGB in the insets

in Figure 7. This is the first reported evidence confirming that when steady state dissolution occurs, the properties of the swollen layer are also constant. Furthermore, there is a noticeable and reproducible peak in the fluorescence intensity at the end of the inner limit of the swollen layer at pH ≥12.5, which is discussed later.

3.5 Fluorescence profiles at high pH (13.5-14)

At higher NaOH concentrations (pH > 13), at room temperature, the dissolution rate is known to decrease with time to very low values (Mercadé-Prieto and Chen 2006; Mercadé-Prieto et al. 2008b). Fluorescence intensity profiles at different times, such as those in Figure 8, did not show the overlap evident in Fig. 7. The limited dissolution at pH > 13 has been attributed to inhibition of swelling by the polyelectrolyte screening effect of the alkali (Mercadé-Prieto et al. 2007c). To date, only overall (macroscopic) swelling data have been available to support this hypothesis.

Mercadé-Prieto and Chen (2006) reported very low dissolution rates for WPC gels in 1 M NaOH. Mercadé-Prieto et al. (2007c) also reported low dissolution rates and little swelling for BLG hydrogels at high pH. Similar findings were obtained with these WPI-RTIC hydrogels (see Supplementary Figures S6 and S7). Therefore, the fluorescence intensity of gels at pH 14 was expected to be close to the initial value because the gels neither swelled nor dissolved. However, Figure 9 shows that the fluorescence intensity dropped dramatically and the affected region increased with time, indicating that the change in fluorescence is marking the volume exposed to alkali. Moreover, the quasi-linear profiles observed in the swollen layer at pH 12-13 (Fig. 7) have been replaced in Figures 8-9 by a strong decay, almost like a step function, indicating that the alkali is influencing the fluorescence of the WPI-RTIC gel. The approach to take into account this effect is described in the next section.

3.6 Quantifying the alkali effect on WPI-RITC fluorescence

The strong influence of pH on the fluorescence evident in Figure 9 was not expected

because the fluorescence of free Rhodamine B (RhB) in water is not affected at alkaline pH (Figure 10). The labelling of proteins with dyes is known to affect their quantum yield due to chemical or steric interactions (Chen 1969). In the current case, the quantum yield, or the fluorescence intensity at constant dye concentration, increases when RITC is covalently linked to whey proteins or in the presence of additional protein (Liu et al. 2017). It is postulated that at high pH these dye-protein interactions could be disrupted and thus lowering the quantum yield. Figure 10 shows that the fluorescence of the WPI-RITC conjugate, without added protein, decreases significantly at pH > 10.

The results in Fig. 10 were obtained at low protein concentrations, whereas in the gels the protein concentration is considerably higher. The effect of protein content on the decrease in fluorescence was studied in the WFM under dissolution-like conditions at constant WPI-RITC concentration. The fluorescence ratio, α, was defined as the ratio of values obtained under alkaline and neutral conditions. The average values of α over the first hour after mixing are plotted against pH in Figure 11. There is a sigmoidal decrease in α with pH between 9 and 13 which was fitted to the expression:

$$\alpha = \alpha_0 + \frac{\Delta\alpha}{1+\exp\left(\frac{p^*-pH}{\Delta p}\right)} \quad (4)$$

where α_0, $\Delta\alpha$, p^* and Δp are fitting parameters listed in Table 1. p^* corresponds to the pK of the transition, and occurs at ~11.6. This value provides insight into why the fluorescence of the WPI-RITC gels decrease with pH: similar pK values were observed in the alkaline denaturation of BLG aggregates (Mercadé-Prieto et al. 2007b), and both values are higher than that reported for the base denaturation of unaggregated BLG, at pH ~10.6 (Taulier and Chalikian 2001). The pK shift in BLG was caused by non-covalent interactions between protein aggregates, and we suggest that similar dye-protein interactions are destroyed here, thereby decreasing the fluorescence intensity.

The results for 10 wt% WPI in Figure 11 differ from the other data sets. Table 1 shows that its $\Delta\alpha$ term is significantly different to the other values. The trends were reproducible, but it was decided to exclude this set from subsequent calculations to

correct the fluorescence data for simplicity. The difference between the values of α at 10 wt% WPI calculated by interpolation (using the sigmoid function parameters from other [WPI] conditions) and the simulated values (using the sigmoid regression parameters at 10 wt%) were used to quantify the uncertainty in α at [WPI] between 5 and 15 wt% ($11 < pH < 13$), resulting with an average relative error of α ~20%.

Above pH 13 the α values decrease further, in a linear manner that cannot be readily represented by the sigmoidal expression (Eqn. (4)): α was therefore calculated using linear interpolation in the interval pH 13-14. The variability of α values at the same pH for different [WPI] is considered as the uncertainty in α with an average absolute error of 0.024. Alkaline induced gelation could occur during the fluorescence measurements, especially when the [WPI] was high (e.g. 15 wt%), but no significant influence of this sol-gel transition on the fluorescence was evident. The fluorescence intensity can also depend weakly on the reaction time (results not presented) and this is accounted for by determining average α values within one hour of contact with alkali. This was considered reasonable as the residence time of the OH^- within the gel before the gel dissolves completely is less than one hour at pH 12-13.

3.7 *Estimation of pH within gels*

Since the aim of this study was to use fluorescence techniques to quantify the local protein content in the swollen gel layer during dissolution, and Fig. 11 shows that fluorescence is strongly affected by both pH and [WPI], the following scheme was devised to account for these effects.

Knowledge of the local pH is required to calculate α but this has not yet been measured inside a dissolving gel. The pH inside the gel was estimated numerically using the Fickian diffusion model for NaOH through protein gels presented by Mercadé-Prieto et al. (2008a), which considers consumption of the alkali due to the titration of the proteins as well as dissolution. A summary of the model is given in the Appendix. The model does not consider changes in the protein concentration - [WPI] is held at the initial value of 15 wt% - so the estimate of the local pH is likely to be poor

when there is substantial swelling. More reliable values are expected at pH 14, when both swelling and dissolution are limited but there is extensive diffusion of OH^- within the gel.

Figure 12(*a*) shows the pH profiles calculated by the model for cases where the dissolution rate is constant, with bulk solution pH 12-13. The calculations employed an effective diffusivity, D_{eff} , of 1.7×10^{-9} m^2 s^{-1} and a constant NaOH penetration thickness with time (δ_{OH}). Both parameters were obtained from the literature for BLG gels using phenolphthalein to visualize the penetration of NaOH at pH ≥ 9.8 (Mercadé-Prieto et al. 2008a). The plots show that the pH changes noticeably within the swollen layer, and values are high as expected, so that correction of α with pH is certainly required when estimating *Q*.

For pH > 13, the dissolution rate is not constant, and therefore δ_{OH} is not constant either. The model was modified to include an initial period in which there was no dissolution (*e.g*. 1 hour in Figure 13(*b*)). In this initial phase the sharp decrease in fluorescence intensity evident in Fig. 8 and 9 should be related to a region where α decreases markedly due to pH, *i.e*. near the pK at pH 11-12. Inspection of the pH and fluorescence profiles shows this to be the case in Figures 12(*b*) and (*c*).

If it is assumed that the steep decrease in fluorescence far from the CGB at pH 13.5 and 14 is only due to pH, e.g. the protein concentration is approximately 15 wt% as there has been little time for dissolution to occur, then the local pH in that part of the gel can be estimated. The results are plotted as dotted lines in Fig.13(*b*) and (*c*). The model parameters, mainly D_{eff}, can be determined from the data, and were adjusted in order to obtain similar pH profiles to the dotted lines. The D_{eff} values obtained, ranging from $1.5\text{-}1.7\times10^{-9}$ m^2 s^{-1}, are in good agreement with previous studies on BLG gels (Mercadé-Prieto et al. 2008a). These results provide confidence in the prediction of local pH for determining α and thus *Q*.

3.8 Corrected Q profiles in gels at high pH

Once the pH profiles within the gel had been obtained, an estimate of the local protein

concentration in the gel is also required in order to calculate the fluorescence correction factor (i.e. α). This was done by solving eq. (3) and (4) iteratively, starting with an initial estimate of [WPI] of 1 wt%. The corrected fluorescence intensity profiles at pH 12-13 are presented in Figure 13(*a*), for locations where the estimated pH was > 11.5. The fluorescence intensity values are now considerably higher (compare with Fig. 7). The *Q* values were calculated (see insets) and close to the CGB the values were 110 ± 20, 25 ± 8 and 11 ± 2 for pH 12, 12.5 and 13, respectively. The corresponding [WPI] values at the interface were 1.3 ± 0.2, 5.6 ± 1.7 and 13 ± 3 wt% (Figure S8). The uncertainties reported consider both the repeatability in I_{WFM} and the uncertainty in α.

Previous research has shown that if the pH is high enough (in practice, between pH 11-12) (Mercadé-Prieto et al. 2007b), and if gels swell above a certain extent, macroscopic dissolution will readily occur, termed 'dissolution threshold' behavior (Mercadé-Prieto et al. 2007a). Critical *Q* values below which macroscopic gels are stable during swelling experiments were estimated at about 23 for similar WPI gels (Li et al. 2016), and around 17 for BLG gels (Mercadé-Prieto et al. 2007a). The *Q* values near the CGB at pH 12 in Figure 13(*a*) are much higher than these but the values at pH 12.5 and 13 are reasonably similar. The existence of a swollen layer with *Q* greater than the critical value at pH 12 and pH 12.5 is possible as dissolution occurs relatively slowly (Fig. 4). The thickness of the high *Q* region is ~0.7 mm at pH 12 and ~0.1 mm at pH 12.5. At pH 13, when dissolution occurs more quickly, the region is very thin and *Q* at the boundary *Q* is close to the critical value.

Figure 13(*b*) shows that at pH 13.5, the corrected fluorescence intensity profiles are statistically the same to that of the initial state ($p>0.05$, Fig. S9(a)), implying limited swelling, with some swelling occurring at the boundary in the subsequent 2 h. At pH 14 (Figure 13(*c*)), where there is little swelling and dissolution, the fluorescence intensity inside the gels remain fairly constant ($p>0.05$, Fig. S9(b)). The average value of *Q* at different times for pH 13.5 is similar (11 ± 2) to the *Q* value for pH 13. At pH 14, the average value of *Q* at different times (16 ± 3) is in good agreement with the value of ~15 reported from macroscopic swelling experiments (Li et al. 2016).

These results demonstrate the capability of WFM to measure *Q* locally in a protein

hydrogel undergoing dissolution and swelling. This is not possible using classical gravimetric or volumetric methods. The pH and the [WPI] dependence of the WPI-RITC fluorescence presents a real challenge for accurate quantification, not only in the determination of the correction factor α, but also in the estimation of the pH inside the gel. For instance, the uncertainty in the intragel pH, which has not been considered here, is affected by the modeling assumption that the [WPI] is constant during the diffusion of NaOH. If the lower [WPI] estimated here were used, faster NaOH diffusion is expected (e.g. less titration reactions and higher diffusivity at lower [WPI]), resulting in slightly higher intragel pH. Therefore, due to α, higher *Q* values should be expected inside the swollen layer, particularly at pH 12-13 (Fig. 13(a)). Close to the gel boundary, where the estimated pH is similar to that of the solutions, *Q* corrections should be minimal. Accurate intragel pH estimations, however, will be only possible if local pH experimental data is ever available.

More reliable estimates with fluorescence techniques will require dye-protein conjugates not affected at the high pHs encountered in cleaning and dissolution studies. It may be noted that a correction was not applied for the swelling-only experiment at pH 11 (Fig. 6). The fluorescence corrections are small at lower pH and low [WPI], as shown in Fig.11. This is confirmed by the integrated fluorescence remaining almost unchanged over the length of the swelling experiment (Fig. S10).

3.9 *Estimated NaOH penetration depth, δ*

The diffusion of OH^- ions is critical in the dissolution of fouling deposits or gels due to their ability to destroy the gel matrix and solubilize proteins (Christian and Fryer 2006). Mercadé-Prieto et al. (2008a) used phenolphthalein to track the diffusion of NaOH into BLG gels as it changes color when pH > 9.8. In our case, the above results reveal a strong alkali effect on the conjugated RITC fluorescence, suggesting that the NaOH penetration depth, δ, could be measured using uncorrected fluorescence intensity profiles. Figure 14 shows schematics of three ways that WFM could be used to

444 determine δ.

445 In Figure 14(*a*) measure δ_1 is the distance between the CGB (determined from
446 bright light microscopy) and the marked point (L_1*), where the fluorescence intensity
447 is equal to the initial value (*i.e.* I_{WFM0}). The location of L_1* was obtained by spline
448 interpolation. Figure 14(*b*) shows the scenario at pH 12.5-14 where a fluorescence peak
449 exists close to the alkali penetration front. Measures δ_2 and δ_3 are the distance between
450 the CGB and the points where the fluorescence intensity is equal to the initial value,
451 located before (L_2*) or after (L_3*) the fluorescence peak, respectively.

452 Figure 15 shows how the NaOH penetration depth measured thus changes with time.
453 At pH 12-13, constant values of δ are observed for both δ_2 and δ_3: this is the regime
454 when the gel dissolves at a constant rate, while at other conditions δ increases
455 continuously with time, with coincidentally similar values observed for pH 11 and 14.
456 The δ_2 values at pH 12.5 and 13 are consistent with those reported for BLG gels
457 visualized by phenolphthalein (i.e. δ_{OH}) (Mercadé-Prieto et al. 2008a), however, much
458 larger values of δ_2 are observed at pH 12. This consistency between δ and δ_{OH}
459 strengthens the confidence in the simulated NaOH concentration results, where δ_{OH} was
460 an input parameter in the calculation (Section 3.7).

461 The above results indicate that the alkaline pH at the fluorescence peak is relatively
462 low (say pH < 10). An unexpected fluorescence peak was also observed during swelling
463 in disc-shaped WPI-RITC gels (Liu et al. 2017). As this peak was only observed when
464 fast swelling occurred, it could be related to anomalous water transport in the gel
465 interior, i.e. shrinkage, decreasing Q. Considering the complex effects of pH and protein
466 concentration on RITC-WPI fluorescence reported above, it is not possible at this stage
467 to exclude that the feature was caused by changes in the quantum yield of the conjugate.

468

469 **4. Conclusions**

470 Wide-field fluorescence microscopy (WFM) has been used to quantify the
471 volumetric swelling ratio Q, e.g. protein content, in hydrogels undergoing swelling and
472 dissolution at room temperature. The hydrogels dissolve readily at pH 12-13, reaching
473 a steady state which is confirmed by the local variation in Q and the size of the swollen

layer. Under strongly alkaline conditions (e.g. pH 14), when dissolution proceeds very slowly, we confirm experimentally that there is very little swelling, which could be the reason for the inhibited dissolution suggested in previous studies. This result might explain why there is an optimum for the cleaning of diary fouling deposits using alkali.

The WFM measurements showed that the highly alkaline conditions cause breakdown of dye-protein interactions that affect the fluorescence of whey proteins conjugated with RITC. A scheme for correcting the effects of alkali and protein concentration was devised and shown to give reasonable results. This allowed us to quantify the protein content within these protein hydrogels under reactive conditions for, to the authors' knowledge, the first time. In addition, we attempt to apply this approach to monitor *in situ* the growth of fouled layer on the surface of heat exchanger in the future, and hopefully to build a quantitative model as well.

APPENDIX

The NaOH concentration profile in a gel is estimated using Fick's first law combined with conservation of mass as reported by Mercadé-Prieto et al. (2008a). This requires numerical evaluation, with length (h) and time intervals (Δt) satisfying

$$\frac{D_{\text{eff}}\Delta t}{h^2} = 0.5 \qquad \text{(eq. A1)}$$

where D_{eff} is the effective diffusivity of NaOH in the gel. The NaOH concentration at a specific depth x and at time $t' = t+\Delta t$ can be estimated from the previous time interval, denoted t, using

$$[OH^-]_{x,t+\Delta t}=0.5([OH^-]_{x-h,t}+[OH^-]_{x+h,t}) \qquad \text{(eq. A2)}$$

During each time interval Δt, the final NaOH concentration that remained in the gel is corrected considering the consumption of acid-base reactions with ionizable

amino acids. The amount of NaOH consumed can be calculated from:

$$[OH^-]_{x,t+\Delta t} - [OH^-]^C_{x,t+\Delta t} = [WPI]_{x,t+\Delta t} \sum_k N_k \left(\frac{1}{1+K_{b,k}[OH^-]^C_{x,t}} - \frac{1}{1+K_{b,k}[OH^-]^C_{x+\Delta t}} \right) \quad \text{(eq. A3)}$$

where the $[OH]^C_{x,t+\Delta t}$ is the corrected final NaOH concentration at position x and time $t+\Delta t$. The protein concentration, $[WPI]_{x,t+\Delta t}$, is calculated considering whey protein as pure β-lactoglobulin (18.4 kDa). The subscript k corresponds to each of the different ionizable residues on the protein at alkaline pH (*i.e*. His, Tyr, Lys, Arg), N_k is the number of units of amino acid k on the protein, and $K_{b,k}$ is the basicity constant for the side chain. The values used in this work were those reported by (Zhao et al. (2016)).

Acknowledgements

This work was supported by the project funding from the Priority Academic Program Development (PAPD) of Jiangsu Higher Education Institution and the "Jiangsu Specially-Appointed Processors Program" of China, the Youth Fund of Natural Science Foundation of Jiangsu Province of China (No. BK20140343), and the National Natural Science Foundation of China, International Cooperation and Exchange Program (21550110192).

References

Alvarez N, Daufin G & Gésan-Guiziou G (2010) Recommendations for rationalizing cleaning-in-place in the dairy industry: Case study of an ultra-high temperature heat exchanger. Journal of Dairy Science. 93(2), 808-821.

Blanpain-Avet P, Andre C, Khaldi M, Bouvier L, Petit J, Six T, Jeantet R, Croguennec T & Delaplace G (2016) Predicting the distribution of whey protein fouling in a plate heat exchanger using the kinetic parameters of the thermal denaturation reaction of beta-lactoglobulin and the bulk temperature profiles. Journal of Dairy Science. 99(12), 9611-9630.

Chen RF (1969) Fluorescent protein-dye conjugates : II. Gamma globulin conjugated with various dyes. Archives of Biochemistry & Biophysics. 133(2), 263-276.

Christian GK & Fryer PJ (2006) The Effect of Pulsing Cleaning Chemicals on the Cleaning of Whey Protein Deposits. Food and Bioproducts Processing. 84(4), 320-328.

English AE, Mafé S, Manzanares JA, Yu X, Grosberg AY & Tanaka T (1996) Equilibrium swelling properties of polyampholytic hydrogels. Journal of Chemical Physics. 104(21), 8713-8720.

Fryer PJ, Christian GK & Liu W (2006) How hygiene happens: Physics and chemistry of cleaning. International Journal of Dairy Technology. 59(2), 76-84.

Ganji F & Vasheghani-Farahani E (2009) Hydrogels in Controlled Drug Delivery Systems. Iranian Polymer Journal. 18(1), 63-88.

Ganji F, Vasheghani-Farahani S & Vasheghani-Farahani E (2010) Theoretical Description of Hydrogel Swelling: A Review. Iranian Polymer Journal. 19(5), 375-398.

Govedarica B, Sovany T, Pintye-Hodi K, Skarabot M, Baumgartner S, Musevic I & Srcic S (2012) Addressing potent single molecule AFM study in prediction of swelling and dissolution rate in polymer matrix tablets. European Journal of Pharmaceutics and Biopharmaceutics. 80(1), 217-225.

Grijspeerdt K, Mortier L, De Block J & Van Renterghem R (2004) Applications of modelling to optimise ultra high temperature milk heat exchangers with respect to fouling. Food Control. 15(2), 117-130.

Huanbutta K, Terada K, Sriamornsak P & Nunthanid J (2013) Advanced technologies for assessment of polymer swelling and erosion behaviors in pharmaceutical aspect. European Journal of Pharmaceutics and Biopharmaceutics. 83(3), 315-321.

Hungerford G, Benesch J, Mano JF & Reis RL (2007) Effect of the labelling ratio on the photophysics of fluorescein isothiocyanate (FITC) conjugated to bovine serum albumin. Photochemical & Photobiological Sciences Official Journal of the European Photochemistry Association & the European Society for Photobiology. 6(2), 152-158.

Laity PR & Cameron RE (2010) Synchrotron X-ray microtomographic study of tablet swelling. European Journal of Pharmaceutics and Biopharmaceutics. 75(2), 263-276.

Laity PR, Mantle MD, Gladden LF & Cameron RE (2010) Magnetic resonance imaging and X-ray microtomography studies of a gel-forming tablet formulation. European Journal of Pharmaceutics and Biopharmaceutics. 74(1), 109-119.

Li H, Zhao L, Chen XD & Mercadé-Prieto R (2016) Swelling of whey and egg white protein hydrogels with stranded and particulate microstructures. International Journal of Biological Macromolecules. 83, 152-159.

Lin C-C & Metters AT (2006) Hydrogels in controlled release formulations: Network design and mathematical modeling. Adv Drug Deliv Rev. 58(12–13), 1379-1408.

Liu WJ, Chen XD & Mercadé-Prieto R (2017) Spatial quantification of hydrogels swelling using wide-field fluorescence microscopy. Chemical Engineering Science. 158, 349-358.

Mahdi Y, Mouheb A & Oufer L (2009) A dynamic model for milk fouling in a plate heat exchanger. Applied Mathematical Modelling. 33(2), 648-662.

Mercadé-Prieto R & Chen XD (2006) Dissolution of whey protein concentrate gels in alkali. AIChE Journal. 52(2), 792-803.

Mercadé-Prieto R, Falconer RJ, Paterson WR & Wilson DI (2007a) Swelling and dissolution of beta-lactoglobulin gels in alkali. Biomacromolecules. 8(2), 469-476.

Mercadé-Prieto R, Paterson WR, Chen XD & Wilson DI (2008a) Diffusion of NaOH into a protein gel. Chemical Engineering Science. 63(10), 2763-2772.

Mercadé-Prieto R, Paterson WR & Wilson DI (2007b) The pH threshold in the dissolution of beta-lactoglobulin gels and aggregates in alkali. Biomacromolecules. 8(4), 1162-1170.

Mercadé-Prieto R, Sahoo PK, Falconer RJ, Paterson WR & Wilson DI (2007c) Polyelectrolyte screening effects on the dissolution of whey protein gels at high pH conditions. Food Hydrocolloids. 21(8), 1275-1284.

Mercadé-Prieto R, Wilson DI & Paterson WR (2008b) Effect of the NaOH Concentration and Temperature on the Dissolution Mechanisms of ß-Lactoglobulin Gels in Alkali. International Journal of Food

581 Engineering. 4(5), 284-290.
582 Natrajan VK & Christensen KT (2009) Two-color laser-induced fluorescent thermometry for microfluidic
583 systems. Measurement Science and Technology. 20(1), 015401.
584 Oztop MH, Rosenberg M, Rosenberg Y, Mccarthy KL & Mccarthy MJ (2010) Magnetic Resonance Imaging
585 (MRI) and Relaxation Spectrum Analysis as Methods to Investigate Swelling in Whey Protein
586 Gels. Journal of Food Science. 75(75), 508-515.
587 Pérez-Mohedano R, Letzelter N & Bakalis S (2015) Development of a swelling-removal model for the
588 scanning fluid dynamic gauge. Food and Bioproducts Processing. 93, 269-282.
589 Paredes JI, Villar-Rodil S, Tamargo-Martínez K, Martínez-Alonso A & Tascón JMD (2006) Real-Time
590 Monitoring of Polymer Swelling on the Nanometer Scale by Atomic Force Microscopy. Langmuir.
591 22(10), 4728-4733.
592 Raccis R, Roskamp R, Hopp I, Menges B, Koynov K, Jonas U, Knoll W, Butt HJ & Fytas G (2011) Probing
593 mobility and structural inhomogeneities in grafted hydrogel films by fluorescence correlation
594 spectroscopy. Soft Matter. 7(15), 7042-7053.
595 Richardson JC, Bowtell RW, Mader K & Melia CD (2005) Pharmaceutical applications of magnetic
596 resonance imaging (MRI). Adv Drug Deliv Rev. 57(8), 1191-1209.
597 Shewan HM & Stokes JR (2014) Review of techniques to manufacture micro-hydrogel particles for the
598 food industry and their applications. Journal of Food Engineering. 119(4), 781-792.
599 Tari O & Pekcan O (2011) Modelling of Swelling by the Fluorescence Technique in Kappa Carrageenan
600 Gels. AIP Conference Proceedings. 1400(1), 470-475.
601 Taulier N & Chalikian TV (2001) Characterization of pH-induced transitions of β-lactoglobulin: ultrasonic,
602 densimetric, and spectroscopic studies. Journal of Molecular Biology. 314(4), 873-889.
603 Wagner D, Burbach J, Grünzweig C, Hartmann S, Lehmann E, Egelhaaf SU & Hermes HE (2016) Solvent
604 and solute ingress into hydrogels resolved by a combination of imaging techniques. The Journal
605 of Chemical Physics. 144(20), 204903.
606 Yassin S, Su K, Lin H, Gladden LF & Axel Zeitler J (2015) Diffusion and Swelling Measurements in
607 Pharmaceutical Powder Compacts Using Terahertz Pulsed Imaging. J Pharm Sci. 104(5), 1658-
608 1667.
609 Zhao L, Chen XD & Mercadé-Prieto R (2016) Understanding the alkali cold gelation of whey proteins
610 with NaCl and SDS. Rheologica Acta. 55(11-12), 909-920.
611
612

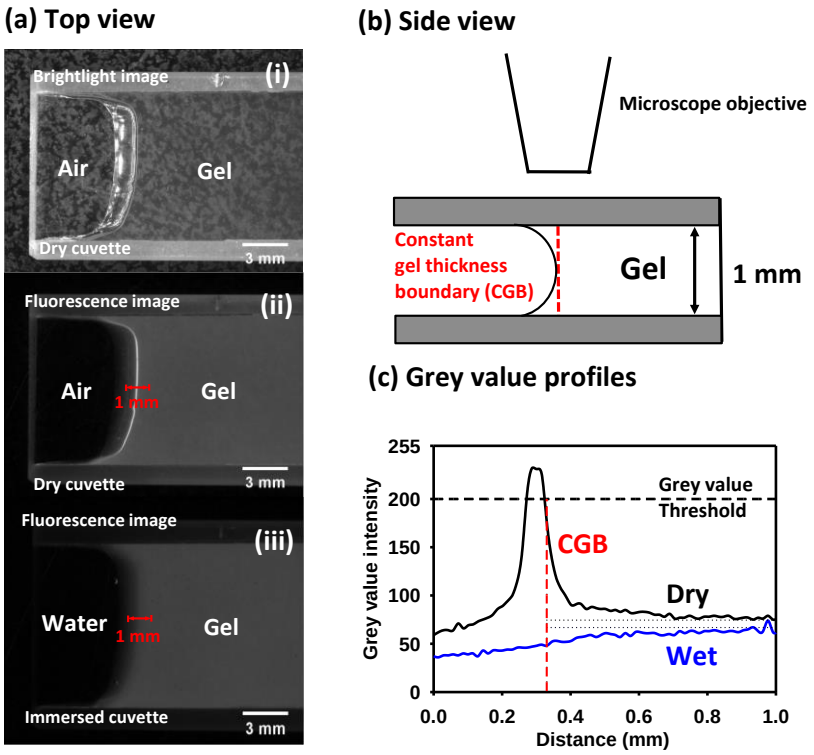

Figure 1. WFM methodology. (*a*) Images of a 15 wt% WPI-RITC gel after gelation: (*i*) bright light, (*ii*) fluorescence, in air, exposure time 8 s, (*iii*) fluorescence, submerged in water, exposure time 8 s; (*b*) Schematic of gel formed in cuvette showing curved boundaries region at wall – dashed vertical line denotes the location of the CGB; (*c*) Variation in grey intensity values along the lines marked in (*a*): Horizontal dotted lines indicate the fluorescence intensity recorded in the interior of the gel, distant from the boundary; black dashed line shows the threshold value applied to a dry image to locate the CGB in an immersed image.

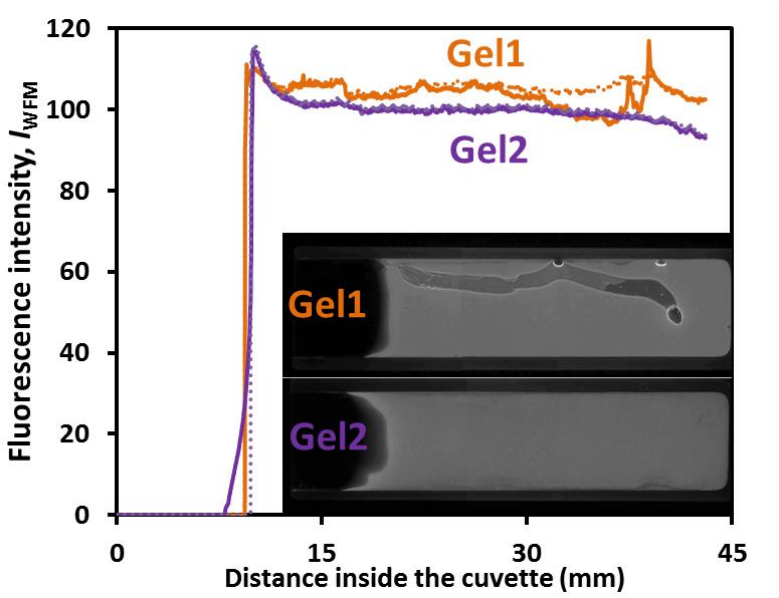

623

624

625 **Figure 2**. Profiles of 1-D fluorescence intensity for 15 wt% WPI-RITC gels after
626 formation. The fluorescence intensity at each location is calculated using the mean grey
627 value (continuous line) and median grey value (dashed line) of the whole width of the
628 gel as outlined in text. Image acquisition condition: magnification 7.13×; exposure time
629 8 s; pixel size ~14 μm.

630

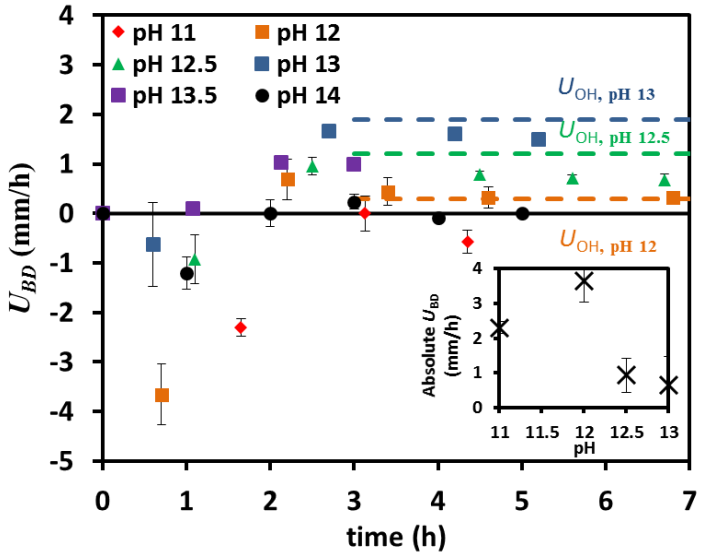

631

632

633 **Figure 3**. Evolution of gel boundary (CBD) velocity for 15 wt% WPI-RITC hydrogels
634 at different pH. Horizontal dashed lines denote the penetration velocity of NaOH into

635 β-lactoglobulin (BLG) gels, U_{OH}, reported by Mercadé-Prieto et al. (2008a). Inset
636 shows the absolute U_{BD} during the initial swelling period (1-2 h). Error bars are the
637 standard deviation (SD) of triplicate experiments.
638

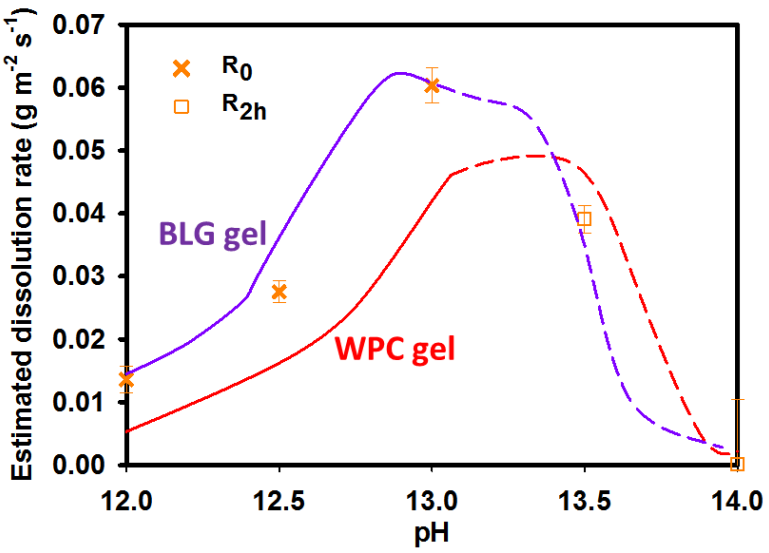

639
640
641 **Figure 4**. Comparison of dissolution rates estimated from U_{BD} data for the WPI-RTIC
642 hydrogels with those reported for whey protein concentrate (WPC) (Mercadé-Prieto
643 and Chen 2006), and β-lactoglobulin (BLG) gels (Mercadé-Prieto et al. 2008b). R_0
644 (solid loci) denotes constant dissolution rates, calculated for experiments where a
645 constant U_{BD} was reached; R_{2h} values (dashed loci) are rates calculated for other cases
646 after 2 h of dissolution, as the rates are not constant with time. Error bars as in Fig. 3.

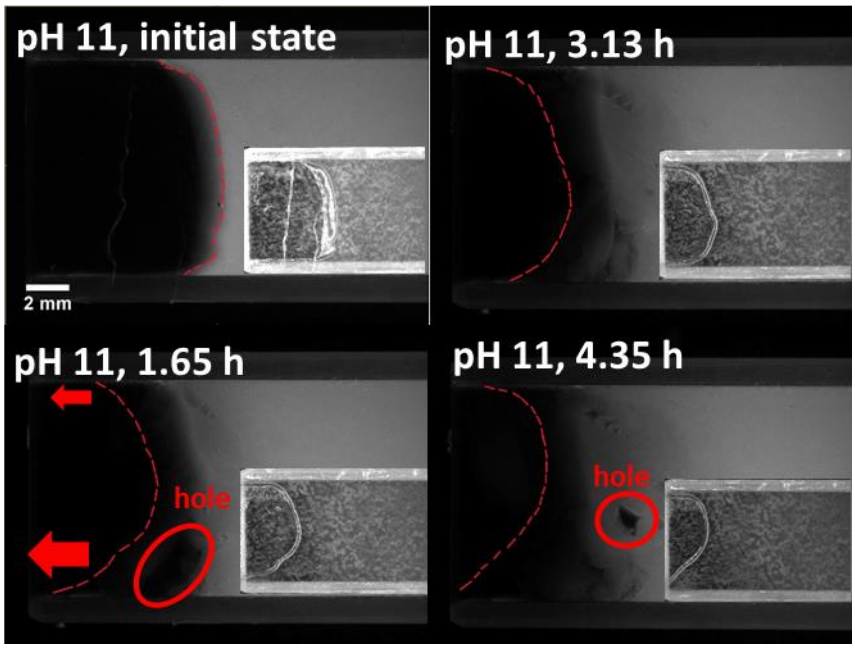

Figure 5. Top view of gels swelling after extended contact at pH 11. Exposure time: 8 s. Insets show bright line images obtained under dry conditions. Red dashed lines denote the estimated CGB location. Length scale common to all frames.

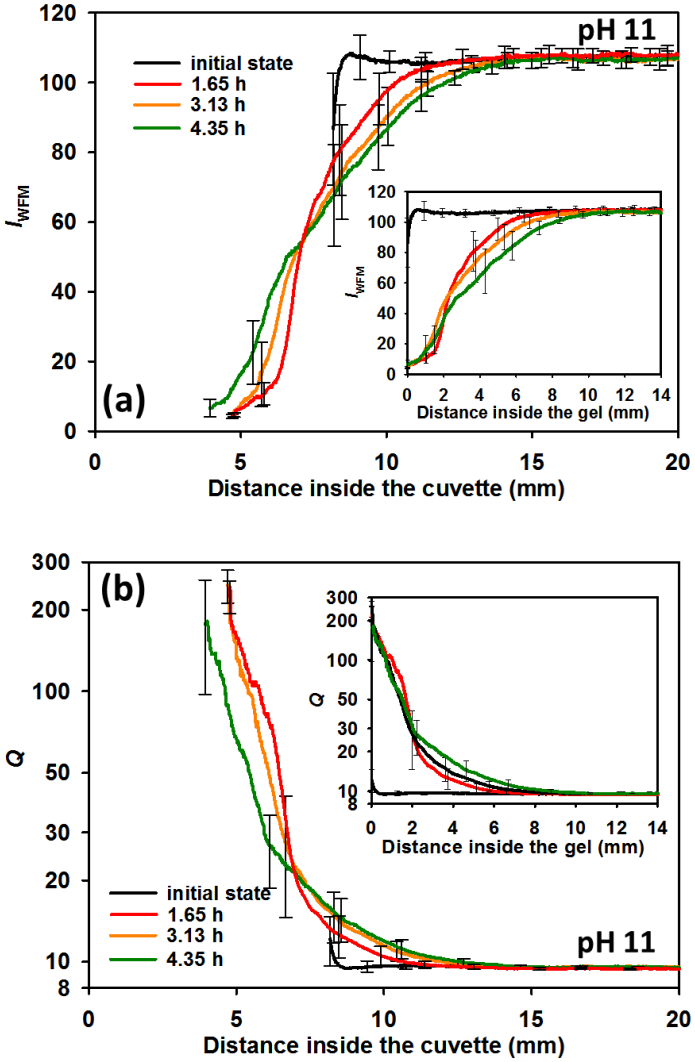

652

653

654 **Figure 6**. Profiles of (*a*) fluorescence intensity, and (*b*) corresponding local swelling
655 ratio for 15 wt% WPI-RITC hydrogels swelling at pH 11. *Q* was calculated using eq. 3.
656 Error bars show SD of triplicates. Insets show the data plotted against distance from
657 CGB. Note the logarithmic scale for *Q* in (*b*).

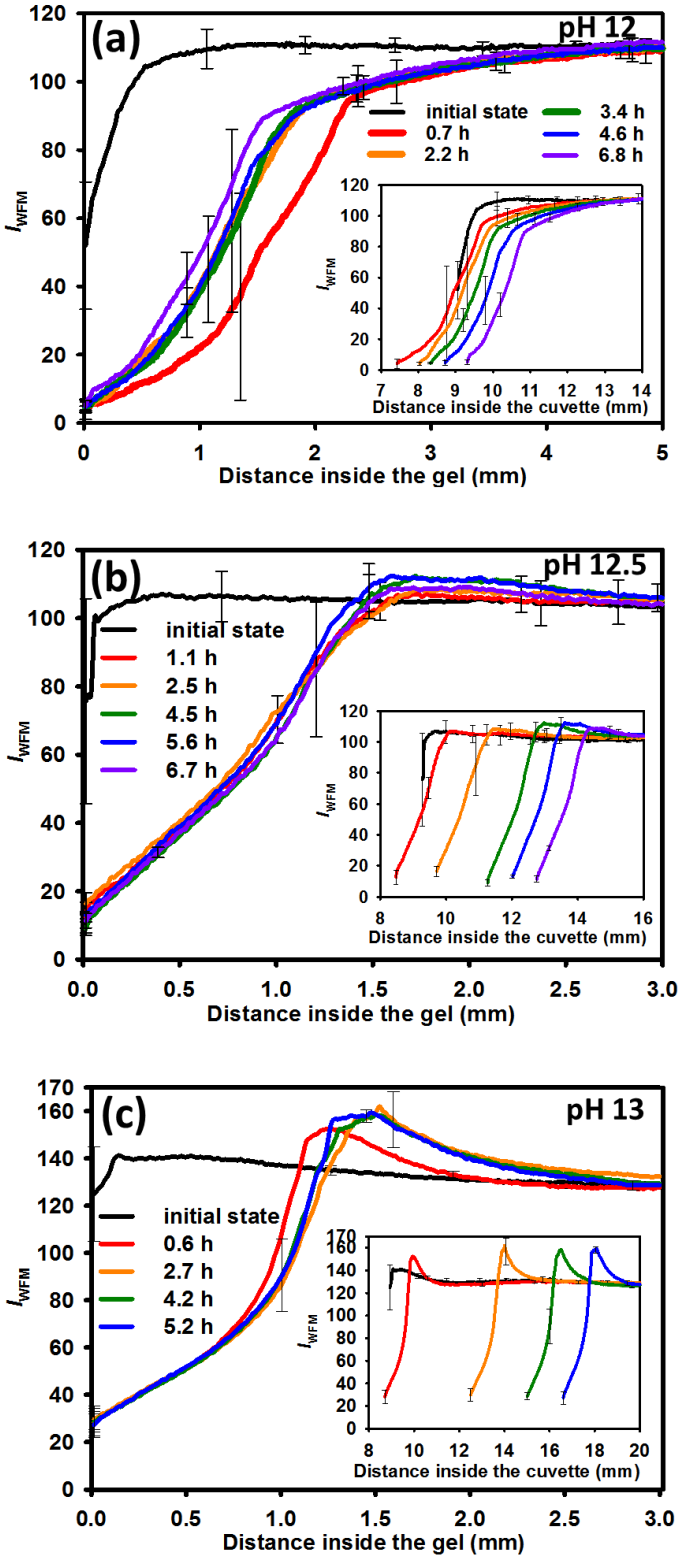

Figure 7. Fluorescence intensity profiles obtained at (*a*) pH 12, (*b*) pH 12.5, and (*c*) pH 13 at different times. Insets show profiles relative to cuvette entrance. Error bars indicate SD of three repeated experiments.

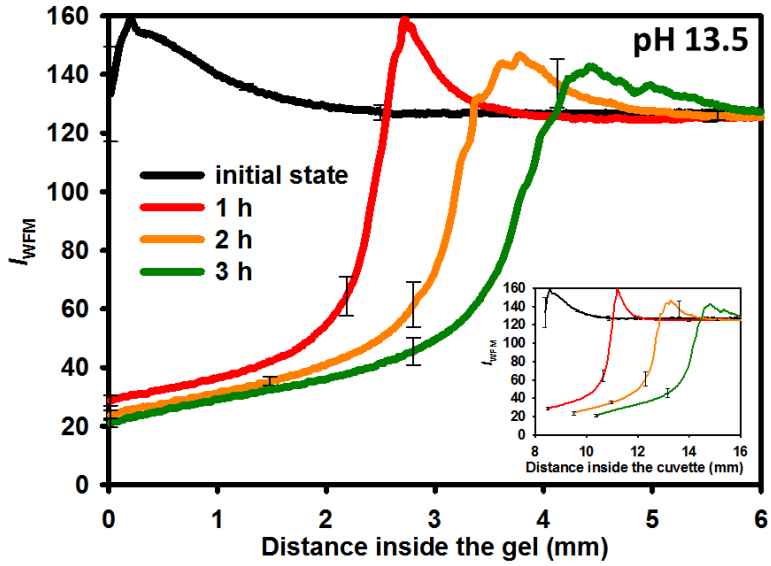

Figure 8. Fluorescence profiles obtained for hydrogels exposed to NaOH solution at pH 13.5 at different times (see legend). Error bars indicate the SD of triplicates. Inset shows fluorescence profiles against distance from the cuvette entrance.

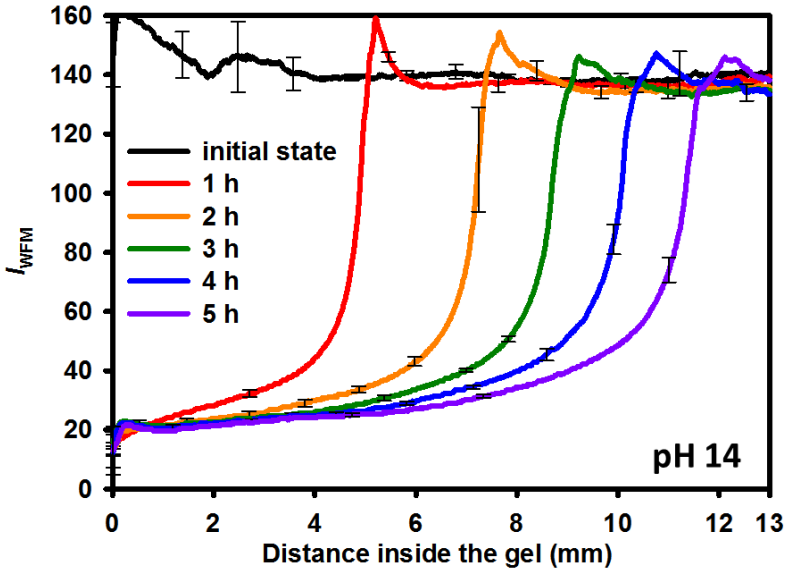

Figure 9. Fluorescence profiles of 15 wt% WPI-RITC hydrogels exposed to NaOH solution at pH 14 for different times (see legend). Error bars show the SD of three repeated experiments.

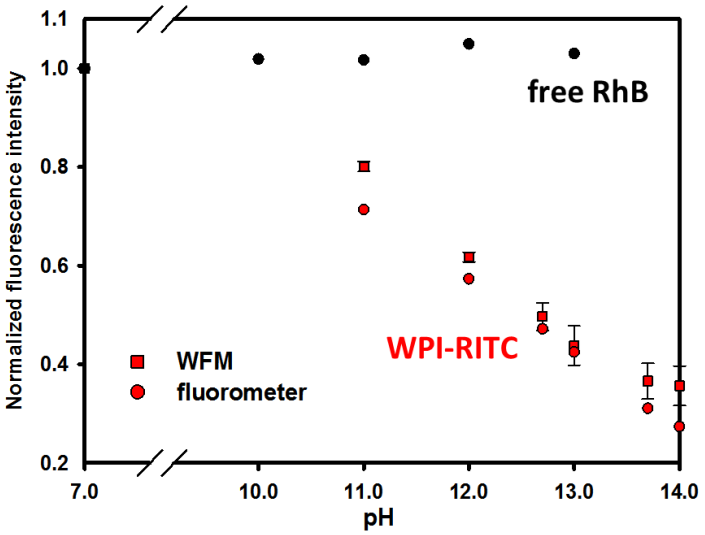

674

675

676 **Figure 10**. Effect of pH on the normalized fluorescence intensity of free RhB and WPI-
677 RITC conjugates. The fluorescence of WPI-RITC was obtained using a fluorometer and
678 by WFM. Fluorometer measurement conditions: excitation 530 nm; emission 580 nm.
679 Error bars for WFM show the SD using three magnifications.

680

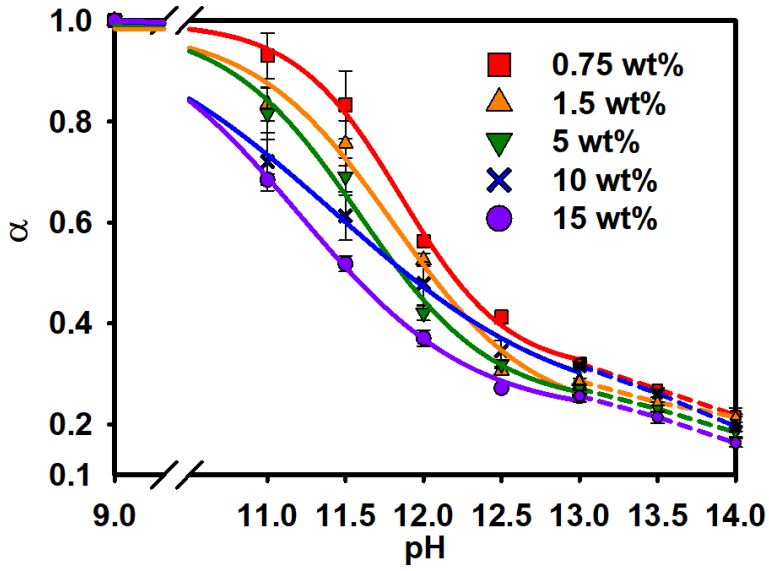

681

682

683 **Figure 11**. Effect of pH on fluorescence ratio α at different native WPI concentrations
684 (shown in legend). Error bars show SDs of α within the first hour of mixing with alkali;

685 for the case of 10 wt% two data sets were used. Solid lines show sigmoidal fit of data
686 to Eq. (4); regression parameters are reported in Table 1. Dotted lines at pH 13-14
687 denote α values estimated by linear interpolation.
688

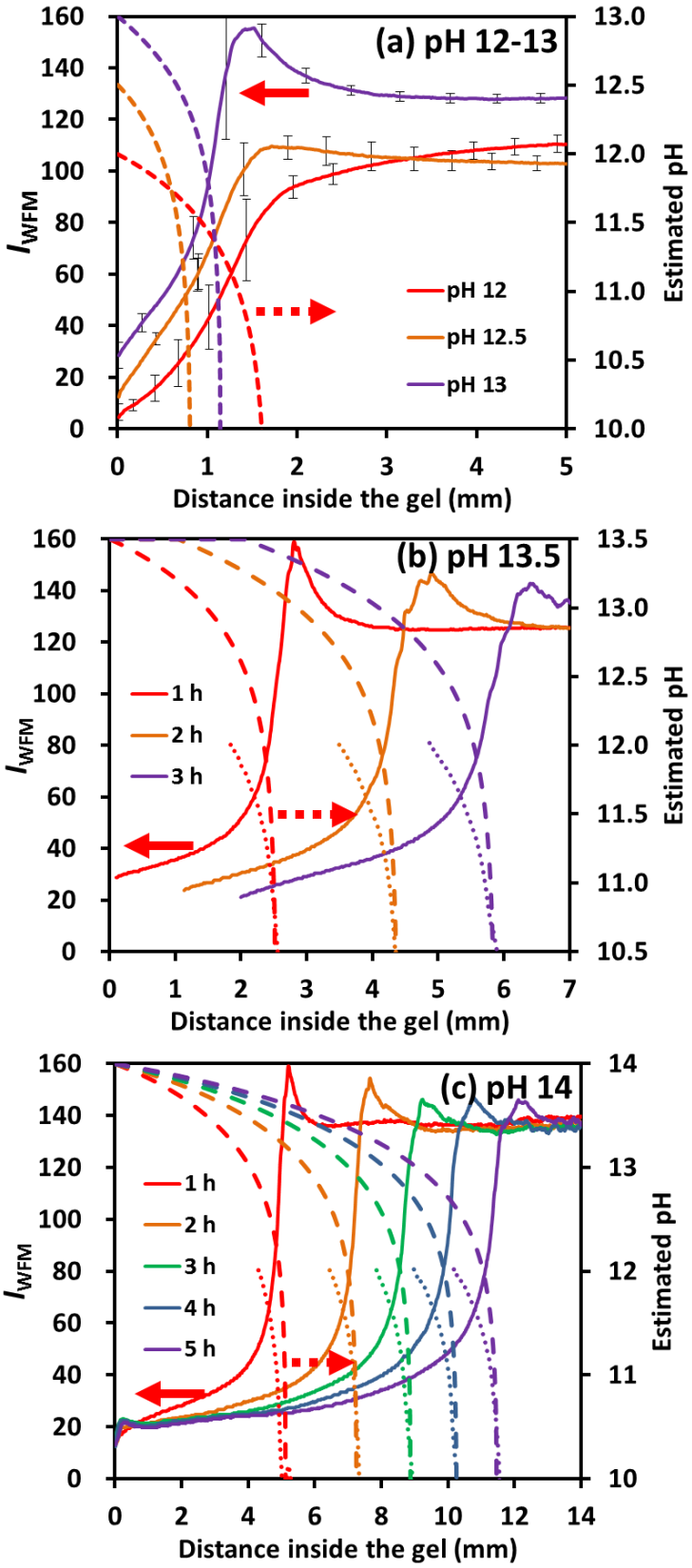

689

690

691 **Figure 12**. Estimated pH profiles and corresponding experimental fluorescence

692 intensity profiles, for 15 wt% WPI-RTIC gels dissolving in NaOH at pH (*a*) 12-13, (*b*)

13.5 and (*c*) 14. The profiles in (*a*) are for steady state conditions, whereas those in (*b*) and (*c*) change over time. Error bars in (*a*) show SDs of overlapping profiles in triplicate experiments. Simulation parameters: (*a*) $D_{eff} = 1.7\times10^{-9}$ m^2 s^{-1}: constant dissolution, δ_{OH} = 1.6, 0.8 and 1.15 mm, for pH 12, 12.5 and 13, respectively (Mercadé-Prieto et al. 2008a). (*b*) No dissolution during the first hour, with $D_{eff} = 0.8\times10^{-9}$ m^2 s^{-1}, followed by uniform dissolution at a rate of 0.017 mm/h with $D_{eff} = 1.5\times10^{-9}$ m^2 s^{-1}. (*c*) No dissolution, $D_{eff} = 1.7\times10^{-9}$ m^2 s^{-1}. Dashed lines denote simulated pH profiles, while dotted lines show the pH profiles calculated assuming that the experimental fluorescence decrease is caused solely by the effect of pH on α.

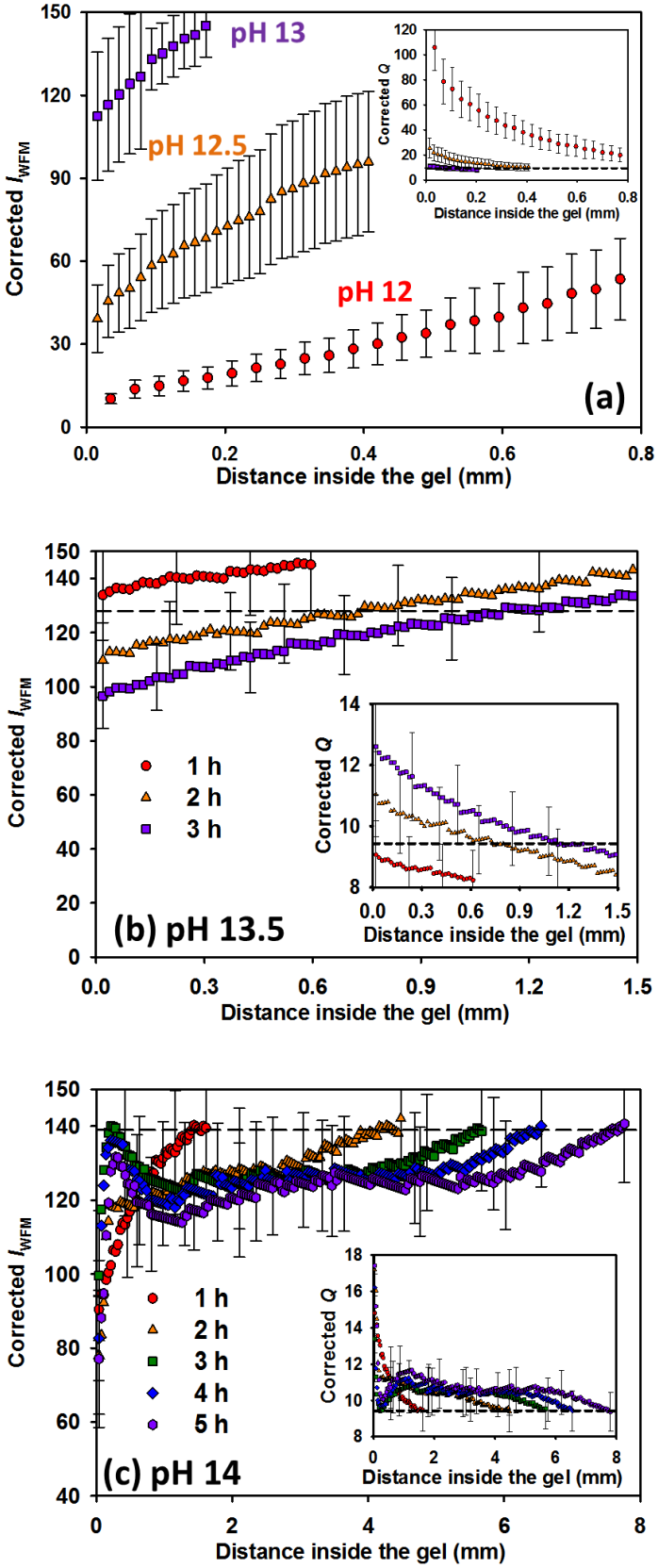

Figure 13. Corrected fluorescence intensity profiles for gels dissolving at pH (*a*) 12-

13, at steady state, and at different times at pH (*b*) 13.5 and (c) 14. Insets show the corresponding swelling ratio profiles. The black dashed lines refer to the fluorescence intensity or Q at formation (Q_r = 9.43). Error bars show uncertainty associated with both the fluorescence intensity and α.

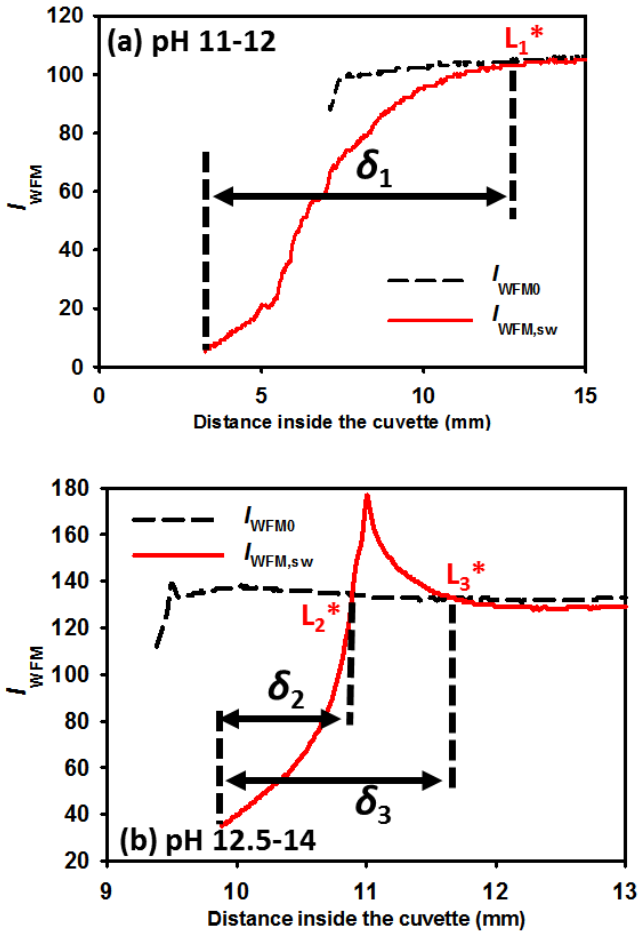

Figure 14. Schematics of measures of NaOH penetration depth based on uncorrected fluorescence profiles. L_1* is the location where the fluorescence intensity is the same as the initial value using spline interpolation. In the cases when fluorescence peak exists, L_2* refers to the value ahead of the peak, while L_3* denotes the value located after the peak.

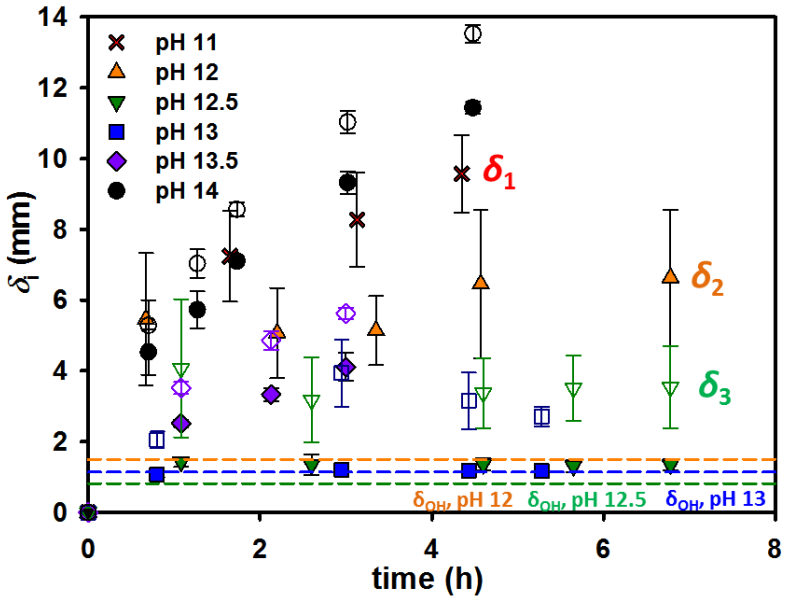

Figure 15. Evolution of estimated NaOH penetration depth for 15 wt% WPI-RITC gels at different pH (see legend), where δ_i was estimated as described in Fig. 14. Error bars show SDs of triplicates. Colored horizontal dashed lines indicate the NaOH penetration depth, δ_{OH}, in BLG gels reported by Mercadé-Prieto et al. (2008a).

Table 1. Parameters obtained by regression fitting data sets in Fig. 11 to eq. (4)

[WPI] (wt%)	α_0	$\Delta\alpha$	p^*	Δp
0.75	0.69±0.04	-0.34±0.05	11.86±0.06	0.30±0.03
1.5	0.77±0.12	-0.45±0.14	11.81±0.17	0.21±0.09
5	0.76±0.07	-0.43±0.09	11.59±0.10	0.24±0.05
10†	0.84±0.11	-0.81±0.17	11.45±0.14	0.19±0.08
15	0.80±0.03	-0.55±0.06	11.21±0.04	0.22±0.02

† Data set not considered in subsequent fluorescence corrections.